UDC 669.24; 620.196.5; 621.791.669
https://doi.org/10.17073/0021-3438-2023-6-44-53

Research article
Научная статья

Structure and properties of welds in electron beam welding of iron-chromium-nickel alloy EP718

S.L. Isaev[1], D.A. Baranov[1], E.Yu. Shchedrin[1], V.S. Muratov[2], K.V. Nikitin[2], S.S. Zhatkin[2]

[1] **JSC "UEC-Kuznetsov"**
29 Zavodskoe shosse, Samara 443022, Russia

[2] **Samara State Technical University**
244 Molodogvardeyskaya Str., Samara 443100, Russia

✉ Konstantin V. Nikitin (kvn-6411@mail.ru)

Abstract: This article presents the results of a study focused on the formation of structural characteristics and properties of welded joints in the EP718 alloy with a 13 mm thickness (accounting for a 3 mm technological substrate). The study explores variations in electron beam welding parameters, such as beam current and the speed of its movement across the specimen's surface, to determine the optimal welding mode for this alloy. This alloy is crucial in the production of high-pressure stators for aircraft engines, as the component operates under low-cycle loads at high stress levels, making its performance critical. Specimens that were welded with a beam speed (v) of 0.0042 m/s and a beam current (*i*) of 85 mA exhibited a minimum tensile strength of 1160 MPa. On the other hand, specimens welded with v = 0.006 m/s and *i* = 65 mA demonstrated a maximum tensile strength of 1270 MPa. However, it's noteworthy that specimens welded at 0.006 m/s with beam currents of 120 mA and 75 mA experienced fracture along the weld, while specimens welded at 0.006 m/s with a beam current of 65 mA and at 0.0042 m/s with a beam current of 85 mA exhibited fracture in the heat-affected zone at a distance of 0.5–3.0 mm from the weld. Examination of the structure of specimens welded at v = 0.006 and 0.0042 m/s and *i* = 120 mA, 75 mA, and 85 mA revealed expanded grain boundaries in the heat-affected zone. Consequently, the optimal welding mode was identified as having a beam speed of 0.006 m/s and a beam current of 65 mA. In this mode, no thickened grain boundaries were detected, and a maximum tensile strength of 1270 MPa was achieved.

Keywords: electron beam welding, heat resistant nickel alloys, heat affected zone, structure, properties.

For citation: Isaev S.L., Baranov D.A., Shchedrin E.Yu., Muratov V.S., Nikitin K.V., Zhatkin S.S. Structure and properties of welds in electron beam welding of iron-chromium-nickel alloy EP718. *Izvestiya. Non-Ferrous Metallurgy.* 2023;29(6):44–53.

https://doi.org/10.17073/0021-3438-2023-6-44-53

Структура и свойства сварных швов при электронно-лучевой сварке железохромоникелевого сплава ЭП718

С.Л. Исаев[1], Д.А. Баранов[1], Е.Ю. Щедрин[1], В.С. Муратов[2], К.В. Никитин[2], С.С. Жаткин[2]

[1] **ПАО «ОДК-Кузнецов»**
Россия, 443022, г. Самара, Заводское шоссе, 29

[2] **Самарский государственный технический университет**
Россия, 443100, г. Самара, ул. Молодогвардейская, 244

✉ Константин Владимирович Никитин (kvn-6411@mail.ru)

Аннотация: Приведены результаты исследований особенностей формирования структуры и свойств сварных соединений сплава ЭП718 толщиной 13 мм (с учетом технологической подкладки 3 мм) за счет варьирования параметров электронно-лучевой свар-

ки (тока луча и скорости его перемещения по поверхности образца) и определения оптимального режима сварки для данного сплава, используемого при изготовлении статора высокого давления авиационного двигателя. Деталь является ответственным крупногабаритным изделием сложной профильной формы и работает в условиях малоцикличных нагрузок при высоком уровне напряжений. Минимальный предел прочности 1160 МПа имеют образцы, сваренные при скорости перемещения луча по поверхности образца v = 0,0042 м/с и токе луча 85 мА. Для образцов, сваренных при v = 0,006 м/с и i = 65 мА, характерен максимальный предел прочности, равный 1270 МПа. При определении временного сопротивления у образцов, сваренных при v = 0,006 м/с, i = 120 и 75 мА, разрушение произошло по сварному шву, а у образцов, сваренных при v = 0,006 м/с, i = 65 мА и v = 0,0042 м/с, i = 85 мА, – по зоне термического влияния на расстоянии 0,5–3,0 мм от сварного шва. При микроисследовании структуры образцов, сваренных при v = 0,006 и 0,0042 м/с и i = 120, 75 и 85 мА соответственно, выявлены расширенные границы зерен в зоне термического влияния. Таким образом, оптимальным является режим сварки при скорости перемещения луча по поверхности образца 0,006 м/с и токе луча 65 мА. На данном режиме утолщенных границ зерен не обнаружено и достигается максимальный предел прочности 1270 МПа.

Ключевые слова: электронно-лучевая сварка, жаропрочные никелевые сплава, зона термического влияния, структура, свойства.

Для цитирования: Исаев С.Л., Баранов Д.А., Щедрин Е.Ю., Муратов В.С., Никитин К.В., Жаткин С.С. Структура и свойства сварных швов при электронно-лучевой сварке железохромоникелевого сплава ЭП718. *Известия вузов. Цветная металлургия*. 2023;29(6):44–53. https://doi.org/10.17073/0021-3438-2023-6-44-53

Introduction

In recent years, the use of heat-resistant alloys in heavy-duty, large-scale power units and assemblies within aviation engineering has significantly expanded. These components often operate under low cycle loads at high stress levels. Among the most compelling alloys are those with tensile strengths ranging from 980 to 1200 MPa [1]. One such alloy, KhN45VMTYUBR-ID (EP718), has gained attention due to its application in parts operating in temperature ranges of up to 700—800 °C. Welding plays a pivotal role in the production of these components.

Welded joints possess distinct mechanical and operational characteristics, which can markedly differ from those of the base metal. The reliability and longevity of welded structures are predominantly influenced by the quality and structure of the weld metal, the heat-affected zone, and the joint's design. Welding heat-resistant alloys introduces unique challenges, including the propensity for defect formation, such as cracks [2; 3].

Electron beam welding (EBW) has emerged as a method offering minimal remelted material, minimal product deformation, and strength on par with the base material. However, achieving high-quality welded joints through EBW requires precise control of edge penetration, as well as minimizing chemical and structural inhomogeneities in the weld metal and heat affected zone (HAZ) while reducing residual stresses and eliminating defects like cracks and pores [4; 5].

Analysis of scientific publications from both foreign and domestic scientists reveals that various methods for creating defect-free permanent joints in the heat-resistant alloy EP718 are actively under investigation worldwide. For example, in [6], defect-free joints on 5 mm thick sheet specimens were achieved using CO_2 laser welding. In another study, laser welding (LW) of 1.3 mm thick EP718 alloy revealed defects in the root part of the weld, such as pores [7]. [8] explored welds of 3.4 mm thick specimens made by additive growth through electric arc welding (EAW) using a non-melting tungsten electrode in a shielding gas environment. Although a fine-grained structure was obtained after heat treatment, cracks were found in the HAZ. In [9; 10], the influence of heat input during electron beam welding on the possibility of eliminating microcracks in the weld and the HAZ of 2 mm thick specimens was investigated. Furthermore, [11—13] examined welds of Inconel 718 heat-resistant alloy produced through EBW, EAW, and LW technologies at various welding modes, showcasing the impact of grain size on mechanical properties. The effects of stirring during friction welding on the mechanical properties of EP718 alloy welds were explored in [14], as were the electric arc modes for welding 2 mm thick specimens [15]. Additionally, [16] delved into the intricacies of weld formation on 3 mm thick specimens using EBW, while [17] analyzed the welding of consumable electrodes by a magnetically compressed arc on 2 mm thick sheet material of the EP718 alloy.

Some publications have focused on investigating the unique aspects related to the geometry and microstructure of welds, as well as the formation of defects in both the weld and the heat-affected zone, examining ultrahigh frequency and conventional EBW, as well as microwave welding [18—20].

In the studies conducted by Russian researchers [21; 22], the structure and properties of welds created through

various welding methods, such as robotic welding with a consumable electrode and LW, were thoroughly examined.

For the fabrication of permanent joints using the heat-resistant alloy KhN45MVTYUBR-ID (EP718), concentrated energy flows, including electron beam welding, show promise due to their ability to produce narrow welds and high-quality joints [23]. Nevertheless, the EBW process comes with its set of challenges and unresolved issues, including the potential for cracks, pores, and other defects within the welded metal, which can compromise the reliability and performance characteristics of the final product [24].

The primary objective of this study was to investigate the specific factors influencing the structure and properties of welded joints crafted from the EP718 alloy, featuring a thickness of 13 mm (accounting for a technological substrate of 3 mm). This was achieved by varying the parameters of electron beam welding, such as beam current and the speed of its movement across the specimen's surface, to identify the optimal welding mode. This alloy is extensively used in the production of high-pressure stators for aircraft engines, where the components are of significant size, possess intricate profiles, and operate under low cycle loads at high stress levels. Remarkably, this study considered these critical operational conditions, which were not always accounted for in previous research [6—22].

Materials and methods

The high-pressure stator is fabricated through the welding of two components: the rear flange, which is constructed from a solid rolled ring following Industry standard OST 1.90396-91, and the middle ring, crafted from EP718 sheet material in accordance with Specifications TU 14-1-5095-92. Following the welding process, the component undergoes heat treatment to relieve stress and attain the necessary mechanical properties.

The investigation of welding parameters and the examination of microstructure and mechanical properties were conducted using simulator specimens measured 200 mm in length, 50 mm in width, and 13 mm in thickness. They are constructed from a solid rolled ring (Fig. 1, loc. *1*) and EP718 heat-resistant alloy sheet material (Fig. 1, loc. *2*).

The local chemical composition of the alloy was assessed through qualitative and quantitative *X*-ray spectral microanalysis using a scanning electron microscope. Spectral analysis was conducted to determine the chemical composition of the specimens, and the results are provided in Table 1. The material grade of the specimens matches the EP718 alloy.

Permanent connections were created using an electron beam welding facility. Various EBW modes were employed, involving adjustments to the specimen's movement speed relative to the beam and the beam current strength.

Following the welding process, the specimens underwent heat treatment. Hardening was conducted in an elevator, and ageing was carried out in a shaft electric furnace. The specific heat treatment modes, including hardening and ageing, are detailed Table 2.

To assess the mechanical properties of welded joints, specimens were prepared based on simulator specimens

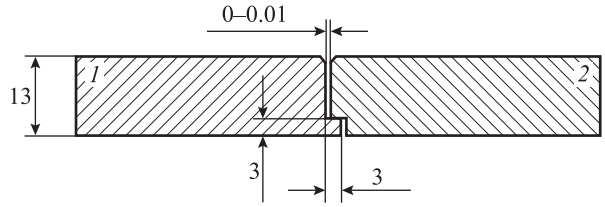

Fig. 1. Sketch of a simulator specimen
1 – solid rolled ring; ***2*** – sheet material
Dimensions are given in mm

Рис. 1. Эскиз образца-имитатора
1 – цельнокатаное кольцо, ***2*** – листовой материал
Размеры указаны в мм

Table 1. **Chemical composition (wt.%) of simulator specimens' material**
Таблица 1. Химический состав (мас.%) материала образцов-имитаторов

Cutting location (Fig. 1)	C	Si	Mn	S	P	Cr	Ni	W	Mo	Ti	Al	Nb
Location 1	0.055	0.007	0.07	0.0016	0.004	15.6	45.24	3.44	4.45	2.08	0.99	1.13
Location 2	0.058	0.08	0.24	0.0016	0.01	15.9	44.73	3.23	4.11	2.17	0.98	1.01
Specifications TU-14-1-5095-92	≤0.1	≤0.3	≤0.6	≤0.01	≤0.015	14–16	43–47	2.5–3.5	4.0–5.2	1.9–2.4	0.9–1.4	0.8–1.5

Table 2. **Heat treatment modes for specimens before and after welding**

Таблица 2. Режимы термической обработки образцов до и после сварки

Heat treatment before welding	Heat treatment after welding		
Quenching	Quenching (stress relieving)	Ageing 1	Ageing 2
t = 1100 °C, τ = 2 h, cooling in air	Heating in air t = 1100 °C, τ = 1 h, cooling to 500–600°C in a container in air with argon supply, further – without argon supply	t = 780 °C, τ = 5 h, cooling in air	t = 650 °C, τ = 16 h, cooling in air

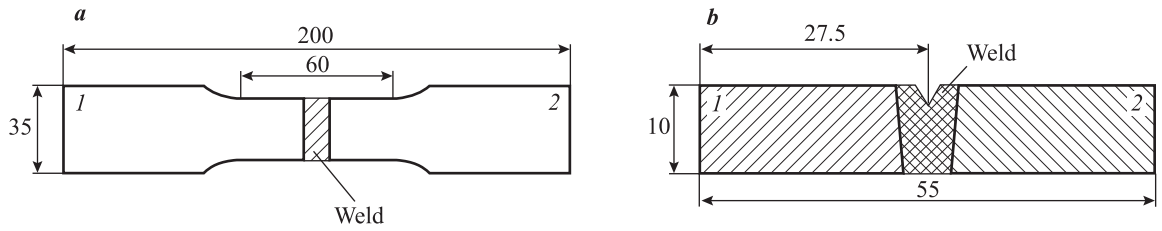

Fig. 2. Sketches of specimens for evaluatng mechanical properties: ultimate tensile strength, yield strength, elongation, and contraction (***a***) and impact strength (***b***)

1 – solid rolled ring, ***2*** – sheet material. Dimensions are given in mm

Рис. 2. Эскизы образцов для оценки механических свойств: временного сопротивления, предела текучести, относительного удлинения и сужения (***a***) и ударной вязкости (***b***)

1 – цельнокатаное кольцо, ***2*** – листовой материал. Размеры указаны в мм

to determine the tensile strength (σ_u), yield strength ($\sigma_{0.2}$), relative elongation (δ), and contraction (ψ) as per State Standard GOST 6996-66 (type XIII, Fig. 2, *a*). Impact strength (*KCU*) was also evaluated in accordance with the standard (type IX, Fig. 2, *b*). Notably, the weld was situated at the center of each specimen.

Grain size was determined by measuring chord lengths in accordance with State Standard GOST 5639-82 using specialized software. Microstructure analysis was conducted using an optical microscope equipped with a solid surface microstructure analyzer at various magnifications. Microhardness measurements were performed under a 50 g load.

Results and discussion

Prior to welding, the tensile strength of specimens from a solid rolled ring was determined to be σ_u = = 930 MPa, while the sheet material exhibited a tensile strength of σ_u = 990 MPa. Due to the higher strength of the latter, which exceeded 980 MPa, a quenching process was carried out before welding. Fig. 3 provides insight into the microstructure of a 13 mm thick sheet of the heat-resistant dispersion-hardening nickel alloy EP718 in its as-delivered state and after quenching at 1100 °C, with a 2-hour hold, followed by air cooling. The microstructure of the base material post-heat treatment consists of austenite grains, carbides, and the γ′ phase (Fig. 3, *a*). In both scenarios, the average grain size falls within the range of 3—6, in accordance with State Standard GOST 5639-82.

A series of simulator specimens was produced under different welding modes (Table 3). These modes involved variations in the speed of beam movement along the specimen's surface (ν) and the beam current (*i*). The selection of these parameters was guided by the specifications and aimed to ensure full penetration of specimens with a thickness of 13 mm. The results of the mechanical tests are provided in Table 4.

In modes *1* and *2*, failure during the determination of time resistance occurred along the weld, whereas in other tested specimens, failure took place in the HAZ at a distance of 0.5—3.0 mm from the weld.

Table 3. **Welding modes**

Таблица 3. Режимы сварки образцов

Mode No.	ν, m/s	*i*, mA
1	0.006	120
2	0.006	75
3	0.006	65
4	0.0042	85

Table 4. **Mechanical properties of welded joints**

Таблица 4. Механические свойства сварных соединений

Mode No.	σ_u, MPa	σ_y, MPa	δ, %	ψ, %	*KCU*, MJ/m^2	Microhardness, kg/mm^2
1	1160	760	17.2	15.5	0.42	308
2	1170	770	17.8	19.0	0.41	329
3	1270	920	21.0	21.7	0.93	348
4	1160	810	15.4	15.5	0.81	335
Specifications TU 14-1-1059-2004	≥1080	≥790	≥13	–	≥0.35	293–363
Specifications TU 14-1-3905-85	≥1080	≥790	≥12	≥14	≥0.35	285–415

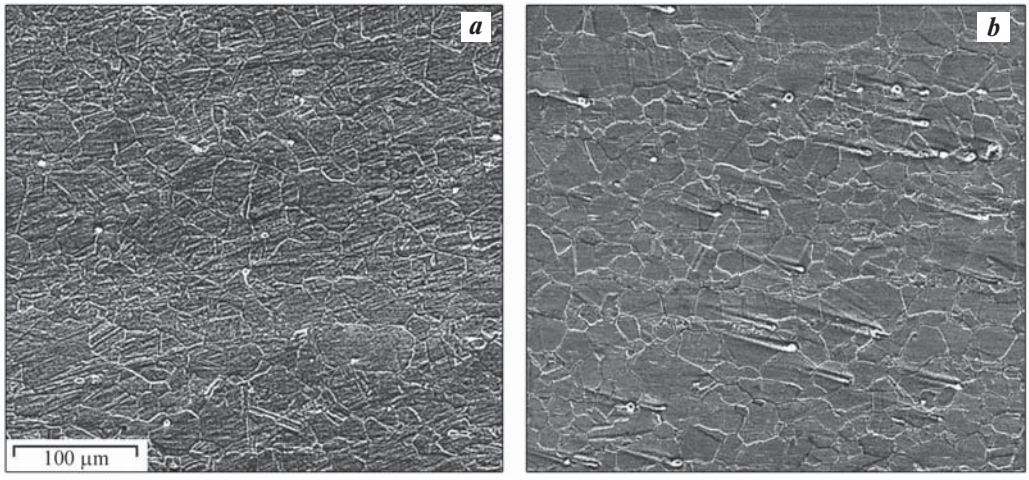

Fig. 3. Microstructure (×400) of EP 718 sheet alloy in as-delivered condition (***a***) and after heat treatment (quenching) (***b***)

Рис. 3. Микроструктура (×400) листового сплава ЭП718 в состоянии поставки (***a***) и после термической обработки (закалки) (***b***)

In the studied welds obtained in modes *1*—*3*, complete penetration was achieved (Fig. 4, *a*—*c*). However, in the welded joint of mode 4, a minor lack of penetration of 0.1 mm was observed, with a single pore of 1.0 mm in diameter detected in one section (indicated by arrows in Fig. 4, *d*). According to specifications (RTM 1.4.1703-87), for this material thickness, pores of up to 1.5 mm are permissible. No cracks or other welding defects were identified during the micro-examination of sections of the welded specimens.

The macrostructure of the welds exhibits characteristic zones associated with EBW, including the "mushroom" zone (dimensions *h* and *b*), the knife zone (*e* and *d*), and the weld root in the locking part of the joints (Fig. 4, *c* and *d*) and in the lining area (Fig. 4, *a*). The overall dimensions of the weld for each mode are presented in Table 5.

The highest weld penetration was achieved at a welding current of 120 mA, while specimens in modes *1*—*3* achieved the required depth. In welding mode *4*, Table 5 shows the widest bath width (*b*) in the 'mushroom' zone and the shallowest depth of penetration. Mode *1* exhibits the highest "mushroom" zone height (*h*), which can lead to additional heating, potential grain boundary thickening, and microcrack formation. Modes *2* and *3* yield the same "mushroom" zone height, but mode *2* has a narrower width. However, mode *3*, with a beam current of 65 mA, provides the shallowest required weld depth, reducing heat input into the metal, minimizing grain boundary thickening in the heat-affected zone, and lowering the risk of crack formation.

In specimens welded in modes *1*, *2*, and *4*, thickened grain boundaries are observed in HAZ before heat treat-

Table 5. **Dimensions of the welds**

Таблица 5. Габаритные размеры сварного шва

Mode No.	*h*, mm	*b*, mm	*e*, mm	*d*, mm	Penetration depth, mm
1	4.0–4.8	8.3–9.0	2.7–3.0	2.1–2.3	13.0
2	3.5–3.7	6.4–7.6	2.6–2.7	2.0–2.3	12.6
3	3.5–3.7	8.0–8.1	2.6–3.0	2.5	11.4
4	4.0–4.6	8.9–9.5	2.7–3.0	0.2–0.8	9.8
Specifications RTM 1.4.1703-87	Optional		1.5–3.5	1.5–2.5	≥10.5

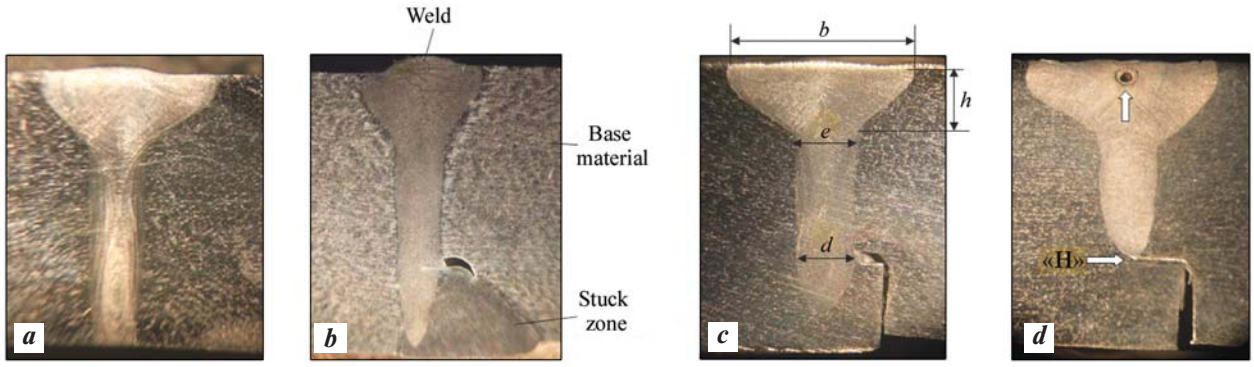

Fig. 4. Macrostructure of welds (×6) obtained in modes ***1*** (***a***), ***2*** (***b***), ***3*** (***c***), and ***4*** (***d***)

Рис. 4. Макроструктура сварных швов (×6), полученных в режимах ***1*** (***a***), ***2*** (***b***), ***3*** (***c***) и ***4*** (***d***)

ment, likely due to carbide phase precipitation during welding and subsequent cooling, accelerating diffusion along grain boundaries, which can lead to crack formation [25]. After heat treatment, the number of thickened grain boundaries increases.

The microstructure of the base material of all specimens is heterogeneous, with varying grain sizes, mainly corresponding to 3—4 points on the GOST 5639-82 scale. In some areas and the heat-affected zone, individual grains with 2—3 points are observed. The microstructure of the specimen from welding mode *3*, shown in Fig. 8, displays no defects in the form of cracks or lack of penetration.

In mode *3*, optimal geometric weld parameters are achieved with no defects. This mode uses the lowest

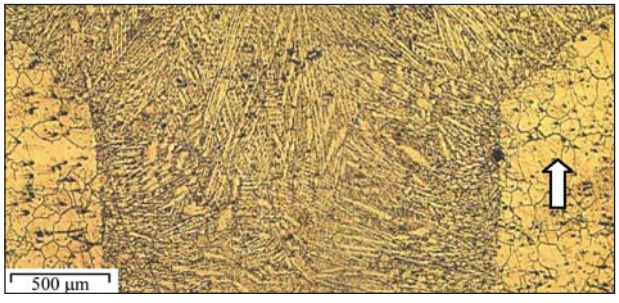

Fig. 5. Microstructure of the weld (×50) obtained in welding mode ***1***

Рис. 5. Микроструктура сварного шва (×50), полученного в режиме сварки ***1***

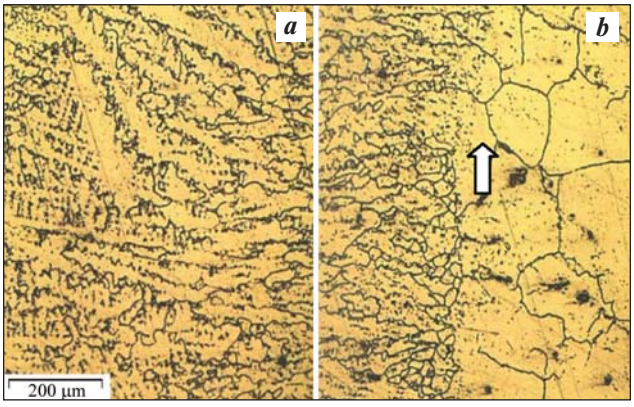

Fig. 6. Microstructure of the specimen (×200) obtained in welding mode ***2***

a – weld, ***б*** – heat-affected zone

Рис. 6. Микроструктура образца (×200), полученного в режиме сварки ***2***

а – сварной шов, ***б*** – околошовная зона

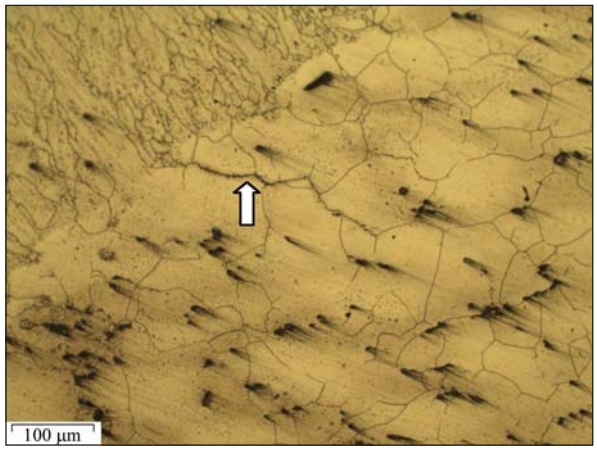

Fig. 7. Microstructure (×100) of the specimen in the heat-affected zone with thickened grain boundaries, obtained in welding mode ***4***

Рис. 7. Микроструктура (×100) образца в околошовной зоне с утолщенными границами зерен, полученного в режиме сварки ***4***

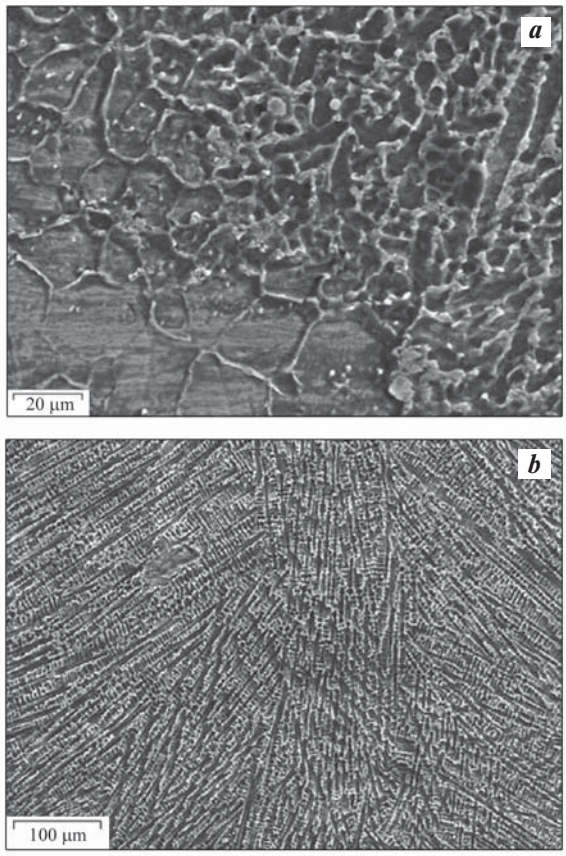

Fig. 8. Microstructure of the base metal sample in the heat-affected zone (***a***) and the weld (***b***) during welding mode ***3***
a –600× magnification, ***b*** – 250× magnification

Рис. 8. Микроструктура образца основного металла в районе околошовной зоны (***a***) и сварного шва (***b***) при сварке в режиме ***3***
a – увеличение 600×, ***b*** – 250×

beam current, which minimizes base material heating while ensuring complete penetration of the edges. The resulting weld exhibits a columnar structure of a cast alloy, with thread-like crystals closer to the center, enhancing the material's heat resistance in the permanent joint.

The intense heat transfer during EBW conditions results in a reduction of the HAZ size and the formation of a fine dendritic structure along the weld's edge (refer to Fig. 8). The base metal in the HAZ maintains a uniform coarse-grained structure, incorporating carbonitrides, carbides, and a finely dispersed intermetallic γ′ phase. In the microstructure of the HAZ, larger grains are observed compared to the base material.

Conclusions

When studying welds in simulator specimens made of the alloy KhN45MVTYUBR-ID (EP718) with a thickness of 13 mm, the following observations were made:

1. The minimum tensile strength of 1160 MPa is recorded in specimens welded at $\nu = 0.0042$ m/s and a beam current (i) of 85 mA (mode *4*). Conversely, specimens welded at $\nu = 0.006$ m/s and $i = 65$ mA (mode *3*) demonstrated a maximum tensile strength of 1270 MPa.

2. Specimens welded at $\nu = 0.006$ m/s, with $i = 120$ and 75 mA (modes *1* and *2*), exhibited fractures along the weld during tensile testing. In contrast, when using welding modes *3* and *4*, destruction was observed along the HAZ at a distance of 0.5—3.0 mm from the weld.

3. Micro-examination of sections from specimens welded in modes *1*, *2*, and *4* revealed expanded grain boundaries in the HAZ.

4. Based on the obtained data, it was determined that welding mode *3*, with parameters $\nu = 0.006$ m/s and $i = 65$ mA, is optimal. This mode exhibited no thickened grain boundaries and achieved an ultimate tensile strength of 1270 MPa.

References

1. Lomberg B.S., Ovsepyan S.V., Bakradze M.M., Mazalov I.S. High-temperature-resistant wrought nickel alloys for advanced gas turbine engines and gas turbine plants. *Vestnik MGTU im. N.E. Baumana. Ser. Mashinostroenie.* 2011;1—10. (In Russ.).
Ломберг Б.С., Овсепян С.В., Бакрадзе М.М., Мазалов И.С. Высокожаропрочные деформируемые никелевые сплавы для перспективных газотурбинных двигателей и газотурбинных установок. *Вестник МГТУ им. Н.Э. Баумана. Сер. Машиностроение.* 2011;1—10.

2. Kablov E.N. Innovative developments of FSUE "VIAM" of the State Scientific Center of the Russian Federation for the implementation of the "Strategic Directions for the Development of Materials and Technologies for Their Processing for the Period up to 2030". *Aviacionnye materialy i tekhnologii*. 2015;1(34):3—33. (In Russ.).
Каблов Е.Н. Инновационные разработки ФГУП «ВИАМ» ГНЦ РФ по реализации «Стратегических направлений развития материалов и технологий их переработки на период до 2030 года». *Авиационные материалы и технологии*. 2015;1(34):3—33.
3. Kablov E.N., Antipov V.V., Sviridov A.V., Gribkov M.S. Features of electron-beam welding of heat-resistant alloys EI698-VD and EP718-ID with steel 45. *Trudy VIAM*. 2020;9(91):3—14. (In Russ.).
https://dx.doi.org/ 10.18577/2307-6046-2020-0-9-3-14
Каблов Е.Н., Антипов В.В., Свиридов А.В., Грибков М.С. Особенности электронно-лучевой сварки жаропрочных сплавов ЭИ698-ВД и ЭП718-ИД со сталью 45. *Труды ВИАМ*. 2020;9(91):3—14.
4. Nazarenko O.K., Kajdalov A.A., Kovbasenko S.N. Electron beam welding red. (Ed. B.E. Paton). Kiev: Naukova dumka, 1987. 256 p. (In Russ.).
Назаренко О.К., Кайдалов А.А., Ковбасенко С.Н. Электронно-лучевая сварка (Под ред. Б.Е. Патона). Киев: Наукова думка, 1987. 256 с.
5. Makarov E.L., Yakushin B.F. Theory of weldability of steels and alloys. Moscow: MGTU im. N.E. Baumana, 2014. 487 p. (In Russ.).
Макаров Э.Л., Якушин Б.Ф. Теория свариваемости сталей и сплавов. М.: МГТУ им. Н.Э. Баумана, 2014. 487 с.
6. Hong J.K., Park J.H., Park N.K., Eom I.S., Kim M.B., Kang C.Y. Microstructures and mechanical properties of Inconel 718 welds by CO_2 laser welding. *Journal of Materials Processing Technology*. 2008;1:515—520.
https://doi.org/10.1016/j.jmatprotec.2007.11.224
7. Patela V., Salia A., Hyderb J., Corlissb M., Hyderb D., Hunga W. Electron beam welding of inconel 718 procedia manufacturing. In: *Proc. 48th SME North American Manufacturing Research Conference* (Ohio, USA). 2020. Vol. 1. P. 428—435.
https://doi.org/10.1016/j.promfg.2020.05.065
8. Raza T., Andersson J., Svensson L.E. Varestraint weldability testing of additive manufactured alloy 718. *Science and Technology of Welding and Joining*. 2018;23(7): 606—611. https://doi.org/10.1080/13621718.2018.1437338
9. Agilan M., Venkateswaran T., Sivakumar D., Pant B. Effect of heat input on microstructure and mechanical properties of Inconel-718 EB welds. *Procedia Materials Science*. 2014;5:656—662.
https://doi.org/ 10.1016/j.mspro.2014.07.312
10. Mei Y., Liu Y., Liu C., Li C., Yu L., Guo Q., Li H. Effect of base metal and welding speed on fusion zone microstructure and HAZ hot-cracking of electron-beam welded Inconel 718. *Materials and Design*. 2016;89:964—977.
https://doi.org/ 10.1016/j.matdes.2015.10.082
11. Peng G., Zhang K.F., Zhang B.G., Jiang S.S., Zhang B.W. Microstructures and high temperature mechanical properties of electron beam welded Inconel 718 superalloy thick plate. *Transactions of Nonferrous Metals Society of China*. 2011;21:315—322.
https://doi.org/ 10.1016/S1003-6326(11)61598-7
12. Manikandan S., Sivakumar D., Rao K.P., Kamaraj M. Effect of enhanced cooling on microstructure evolution of alloy 718 using the gas tungsten arc welding process. Weld World. 2016. 18 p.
https://doi.org/10.1007/s40194-016-0349-1
13. Zhang Y.N., Cao X., Wanjara P. Microstructure and hardness of fiber laser deposited Inconel 718 using filler wire. *The International Journal of Advanced Manufacturing Technology*. 2013;69:9—12.
https://doi.org/10.1007/s00170-013-5171-y
14. Song K.H., Kim W.Y., Nakata K. Investigation of microstructure and mechanical properties on surface-modified Inconel 718 alloy. *Materials Transactions*. 2013;(54)10:2032—2036.
https://doi.org/10.2320/matertrans.M2013096
15. Sonar T., Balasubramanian V., Malarvizhi S., Venkateswaran T., Sivakumar D. Effect of Delta current and Delta current frequency on microstructure and tensile properties of gas tungsten constricted arc (GTCA) welded Inconel 718 alloy joints. *Journal of the Mechanical Behavior of Materials*. 2019;28(1):186—200.
https://doi.org/10.1515/jmbm-2019-0020
16. Sumit K. Sharma, Prashant Agarwal, J. Dutta Majumdar. Studies on electron beam welded Inconel 718 similar joints: Proceedings of the International Conference on Sustainable Materials Processing and Manufacturing (23—25 January 2017, Kruger National Park). *Procedia Manufacturing*. 2017;7:654—659. https://doi.org/10.1016/j.promfg.2016.12.097
17. Tushar S., Visvalingam B., Sudersanan M., Thiruvenkatam V., Dhenuvakonda S. Influence of magnetically constricted arc traverse speed (MCATS) on tensile properties and microstructural characteristics of welded Inconel 718 alloy sheets. *Defence Technology*. 2020. P. 40.
https://doi.org/10.1016/j.dt.2020.07.009
18. Kwon S.I., Bae S.H., Do J.H., Jo C.Y., Hong H.U. Characterization of the microstructures and the cryogenic mechanical properties of electron beam welded Inconel 718. *Metallurgical and Materials Transactions*. 2015;47(2):77—87.
https://doi.org/10.1007/s11661-015-3269-6
19. Jia Z., Wan X., Guo D. Study on microstructure and me-

chanical properties of Inconel718 components fabricated by UHFP-GTAW technology. *Materials Letters*. 2019;261:1—9. https://doi.org/10.1016/j.matlet.2019.127006

20. Bansal A., Sharma A.K., Das S., Kumar P. Characterization of microstructure and strength of microwave welded Inconel 718 joints at 2.45 GHz frequency. *Kovove materialy*. 2016;54:27—35. https://doi.org/10.4149/km_2016_1_27
21. Nikiforov R.V., Galimov V.R., Hisamutdinov E.R., Kamaletdinova R.R., Basharov R.R. Structure and properties of welded joints of EP718 alloy produced by robotic consumable electrode welding. *Vestnik UGATU*. 2021;4(94):10—18. (In Russ.).
Никифоров Р.В., Галимов В.Р., Хисамутдинов Э.Р., Камалетдинова Р.Р., Башаров Р.Р. Структура и свойства сварных соединений сплава ЭП718, полученных роботизированной сваркой плавящимся электродом. *Вестник УГАТУ*. 2021;4(94):10—18.
22. Baranov D.A., Parkin A.A., Zhatkin S.S. Peculiarities of weld seam formation in KhN45VMTYuBR heat-resistant alloy depending on laser welding modes. *Izvestiya Samarskogo nauchnogo centra Rossiyskoy akademii nauk*. 2018;4(2):170—176. (In Russ.).
Баранов Д.А., Паркин А.А., Жаткин С.С. Особенности формирования сварного шва жаропрочного сплава ХН45ВМТЮБР в зависимости от режимов лазерной сварки. *Известия Самарского научного центра Российской академии наук*. 2018;4(2):170—176.
23. Kaydalov A.A. Electron beam welding and related technologies. Kiev: Ekotekhnologiya, 2004. 260 p. (In Russ.).
Кайдалов А.А. Электронно-лучевая сварка и смежные технологии. Киев: Экотехнология, 2004. 260 с.
24. Sorokin L.I. Formation of hot cracks in the near-weld zone during welding of heat-resistant nickel alloys. *Svarochnoe proizvodstvo*. 2005;8:4—18. (In Russ.).
Сорокин Л.И. Образование горячих трещин в околошовной зоне при сварке жаропрочных никелевых сплавов. *Сварочное производство*. 2005;8:4—18.
25. Parshukov L.I., Gilmutdinov F.Z. Electron-beam welding and local heat treatment of welds from heat-resistant alloys. *Trudy VIAM*. 2017;5(53):23—31. (In Russ.). http://dx.doi.org/10.18577/2307-6046-2017-0-5-3-3
Паршуков Л.И., Гильмутдинов Ф.З. Электронно-лучевая сварка и локальная термообработка сварных швов из жаропрочных сплавов. *Труды ВИАМ*. 2017;5(53):23—31.

Information about the authors

Sergey L. Isaev – Deputy Chief Welder for Production, PJSC "ODK-Kuznetsov".
https://orcid.org/0009-0006-6329-4685
E-mail: isl231083@yandex.ru

Dmitry A. Baranov – Cand. Sci.(Eng.), Deputy Chief Welder for New and Repair Technologies, PJSC "ODK-Kuznetsov".
https://orcid.org/0009-0009-8955-8556
E-mail: D.Baranov91@mail.ru

Evgeny Yu. Shchedrin – Chief Welder, PJSC "ODK-Kuznetsov".
https://orcid.org/0009-0004-0406-915X
E-mail: Chiefwelder24@yandex.ru

Vladimir S. Muratov – Dr. Sci. (Eng.), Professor of the Department of Metallurgy, Powder Metallurgy, Nanomaterials, Samara State Technical University (SamSTU).
https://orcid.org/0000-0001-8637-1096
E-mail: muratov1956@mail.ru

Konstantin V. Nikitin – Dr. Sci. (Eng.), Dean of the Faculty of Metallurgy, Mechanical Engineering and Transport, SamSTU.
https://orcid.org/0000-0001-7061-0144
E-mail: kvn-6411@mail.ru

Sergey S. Zhatkin – Cand. Sci.(Eng.), Professor of the Department of Foundry and High-Efficiency Technologies, SamSTU.
https://orcid.org/0000-0001-5625-848X
E-mail: Sergejat@mail.ru

Информация об авторах

Сергей Леонидович Исаев – зам. гл. сварщика по производству, ПАО «ОДК-Кузнецов».
https://orcid.org/0009-0006-6329-4685
E-mail: isl231083@yandex.ru

Дмитрий Александрович Баранов – к.т.н., зам. гл. сварщика по новым и ремонтным технологиям, ПАО «ОДК-Кузнецов».
https://orcid.org/0009-0009-8955-8556
E-mail: D.Baranov91@mail.ru

Евгений Юрьевич Щедрин – гл. сварщик, ПАО «ОДК-Кузнецов».
https://orcid.org/0009-0004-0406-915X
E-mail: Chiefwelder24@yandex.ru

Владимир Сергеевич Муратов – д.т.н., профессор кафедры «Металловедение, порошковая металлургия, наноматериалы», Самарский государственный технический университет (СамГТУ).
https://orcid.org/0000-0001-8637-1096
E-mail: muratov1956@mail.ru

Константин Владимирович Никитин – д.т.н., декан факультета металлургии, машиностроения и транспорта, СамГТУ.
https://orcid.org/0000-0001-7061-0144
E-mail: kvn-6411@mail.ru

Сергей Сергеевич Жаткин – к.т.н., профессор кафедры «Литейные и высокоэффективные технологии», СамГТУ.
https://orcid.org/0000-0001-5625-848X
E-mail: Sergejat@mail.ru

Contribution of the authors

S.L. Isaev – determined the purpose of the work, conducted experiments, wrote an article.

D.A. Baranov – prepared the initial samples, participated in the discussion of the results.

E.Yu. Shchedrin – participated in the metallographic study of the structure of welds, participated in the discussion of the results.

V.S. Muratov – determined the methodology of experiments, participated in the discussion of the results, wrote the article.

K.V. Nikitin – participated in writing the article and discussing the results

S.S. Zhatkin – carried out a literature review, participated in the discussion of the results.

Вклад авторов

С.Л. Исаев – определение цель работы, проведение экспериментов, написание текста статьи.

Д.А. Баранов – подготовка исходных образцов, участие в обсуждении результатов.

Е.Ю. Щедрин – участие в проведении металлографического исследования структуры сварных швов и в обсуждении результатов.

В.С. Муратов – определение методики экспериментов, участие в обсуждении результатов, написание текста статьи.

К.В. Никитин – участие в написании статьи и обсуждении результатов

С.С. Жаткин – литературный обзор, участие в обсуждении результатов.

The article was submitted 11.07.2023, revised 02.10.2023, accepted for publication 04.10.2023

Статья поступила в редакцию 11.07.2023, доработана 02.10.2023, подписана в печать 04.10.2023